


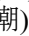





High-Performance Microwave Frequency Standard Based on Sympathetically Cooled Ions

Hao-Ran Qin (秦浩然)^{1,2} Sheng-Nan Miao (苗胜楠)¹ Ji-Ze Han (韩济泽)¹
Nong-Chao Xin (辛弄潮)¹ Yi-Ting Chen (陈一婷)¹ J.W. Zhang (张建伟)^{1,*}
and L.J. Wang (王力军)^{1,2,†}

¹State Key Laboratory of Precision Measurement Technology and Instruments, Key Laboratory of Photon Measurement and Control Technology of Ministry of Education, Department of Precision Instrument, Tsinghua University, Beijing 100084, China

²Department of Physics, Tsinghua University, Beijing 100084, China

 (Received 15 April 2022; revised 7 June 2022; accepted 22 June 2022; published 8 August 2022)

The ion microwave frequency standard is a candidate for the next generation of microwave frequency standard with the potential for very wide applications. The Dick effect and second-order Doppler frequency shift (SODFS) limit the performance of ion microwave frequency standards. The introduction of sympathetic cooling technology can suppress the Dick effect and SODFS and improve the stability and accuracy of the frequency standard. However, the sympathetically cooled ion microwave frequency standard has seldom been studied before. This paper reports a high-performance sympathetically cooled ion microwave frequency standard in a Paul trap. Using laser-cooled $^{40}\text{Ca}^+$ as coolant ions, $^{113}\text{Cd}^+$ ion crystal is cooled to below 100 mK and has a coherence lifetime of over 40 s. The short-term frequency stability reached $3.48 \times 10^{-13}/\tau^{1/2}$, which is comparable to that of the mercury ion frequency standard. Its uncertainty is 1.5×10^{-14} , which is better than that of directly laser-cooled cadmium ion frequency standard.

DOI: [10.1103/PhysRevApplied.18.024023](https://doi.org/10.1103/PhysRevApplied.18.024023)

I. INTRODUCTION

Faced with long-distance, short-duration, and high-speed situations, atomic clocks play an extremely useful role in basic science and practical applications. Because of their compact volume and mature technology, microwave frequency standards are widely used in satellite navigation [1,2], telecommunications [3], timekeeping [4,5], and space exploration [6–8]. Trapped-ion clocks constitute promising candidates for the next-generation microwave atomic clocks due to the advantages of compactness, high transportability, and high performance. To date, ion frequency standards based on $^{199}\text{Hg}^+$ [5,6,9,10], $^{113}\text{Cd}^+$ [11–13], $^{171}\text{Yb}^+$ [14–16] have brought about considerable progress.

Soon after laser cooling technology was proposed [17, 18] and realized [19,20], it was quickly and widely applied in atomic clock devices [21]. Fountain clocks based on ultracold cesium atoms play a role in establishing primary frequency standards of the SI (the International System of Units) second [22]. Optical clocks based on laser-cooled single ion or atoms in optical lattice are expected to

feature in establishing the next-generation definition of the second [23].

Previously, the lack of a suitable electric dipole transition energy level or a laser capable of generating a suitable wavelength had limited the use of some atomic particles that could not be directly laser cooled. As a result, sympathetic cooling was introduced into the field of atomic clocks [24–27]. With relative uncertainties below 10^{-18} , single ion of $^{27}\text{Al}^+$ sympathetically cooled by $^{25}\text{Mg}^+$ underlie the most accurate optical atomic clocks built so far [24].

Nevertheless, the frequency standard based on laser-cooled trapped ions usually suffers from the Dick effect because of the dead time in the laser-cooling process and second-order Doppler frequency shift (SODFS) introduced by the ions rising temperature during interrogation. These limitations can be overcome by sympathetic cooling. However, prior to our work, the only sympathetically cooled ion microwave frequency standard realized was that constructed by Bollinger and colleagues using a Penning trap with Be^+ sympathetically cooled by Mg^+ [28]. A ion ensemble of sympathetically cooled Be^+-Ca^+ in permanent-magnet Penning trap also shows the potential to become a portable atomic clock [29]. In past work, we have demonstrated the laser-cooled cadmium ion

*zhangjw@tsinghua.edu.cn

†lwang@tsinghua.edu.cn

microwave frequency standard [11–13], and have made much progress in sympathetically cooled large ion crystals [30–32].

In this work, we report the realization of a high-performance microwave frequency standard based on sympathetically cooled cadmium ions. Approximately 5000 $^{113}\text{Cd}^+$ ions are trapped in a linear Paul trap and are sympathetically cooled to below 100 mK with $^{40}\text{Ca}^+$, forming a large two-component ion crystal. This frequency standard exhibits a short-term fractional frequency stability of $3.48 \times 10^{-13}/\tau^{1/2}$ (where τ is the averaging time), obtained when serving a crystal oscillator with Ramsey interrogation measurements of 5-s duration, with a fractional accuracy of 1.5×10^{-14} . Compared with a hydrogen maser, the short-term stability of the clock signal is indirectly measured to be $1.36 \times 10^{-13}/\tau^{1/2}$ obtained because of the ultralong Ramsey free evolution time of 50 s, which, encouragingly, ensures future improvements in performance.

II. REALIZATION OF SYMPATHETIC COOLING

In our work, we choose laser-cooled (LC) $^{40}\text{Ca}^+$ as coolant ions and sympathetically cooled (SC) $^{113}\text{Cd}^+$ as “clock” ions. The relevant energy-level structure of cadmium and calcium are shown in Fig. 1. The ground-state hyperfine splitting frequency (15.2 GHz) of the $^{113}\text{Cd}^+$ is the second largest among all working energy levels of atomic microwave clocks, only to $^{199}\text{Hg}^+$ with a frequency of 40.5 GHz. The 800-MHz $^2P_{3/2}$ -state hyperfine splitting ensures that only one laser is needed to complete the state preparation and detection. Therefore, the $^{113}\text{Cd}^+$ frequency standard has promise for high performance in application as well as potential for miniaturization in fabrication. We adopt $^{40}\text{Ca}^+$ as coolant ions because the natural abundance of ^{40}Ca is as high as 97%, and hence easily available. Moreover, the laser providing the cooling is also readily available. Compared with previously used $^{24}\text{Mg}^+$ [30], $^{40}\text{Ca}^+$ has a closer mass to $^{113}\text{Cd}^+$, which facilitates sympathetic cooling.

The core of the whole system is a linear quadrupole trap (see Fig. 2). Each electrode is divided into three segments: the middle segment with length of 40 mm that acts as rf electrodes for radial confinement, and the two ends of length 20 mm that act as end-cap (EC) electrodes for axial confinement [31,32]. The radius of each electrode is $r_e = 7.1$ mm and the distance to the main central axis of the trap is $r_0 = 6.2$ mm to obtain the most ideal quadrupole field and to reduce rf heating [33]. We use a precision-voltage reference chip and a trimming potentiometer to control the dc compensation voltage on the electrodes, miniaturizing the micromotion of trapped ions. The ion trap is installed in a vacuum chamber [31]. Using an ion pump and a titanium sublimation pump, the pressure in the vacuum chamber is below 10^{-9} Pa, which reduces the

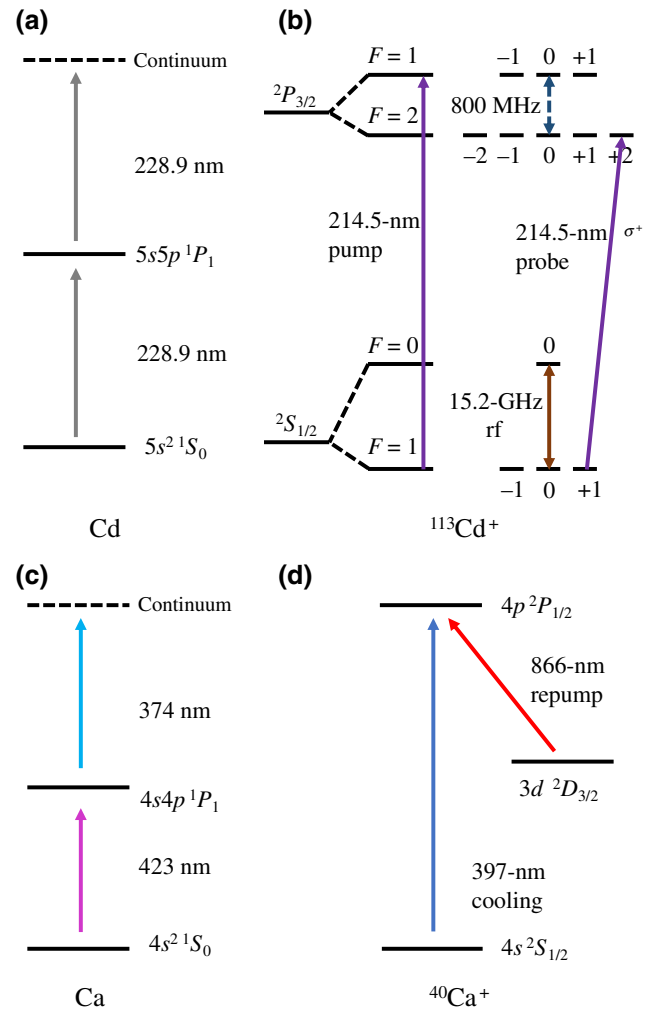


FIG. 1. Relevant energy-level structure of cadmium and calcium: (a),(c) are the energy-level structures of neutral atoms, while (b),(d) are those of isotopic ions. The frequency or wavelength of the electromagnetic wave associated with each transition is given.

frequency shift and decoherence introduced by collision between ions and background gas molecules. A six-layer magnetic shielding barrel is installed on a liftable stage, which not only ensures good magnetic shielding, but also facilitates installation and adjustments.

The schematic of the entire experimental system is shown in Fig. 2. We use a tunable diode laser operating at a wavelength of 423 nm and a single-mode diode laser operating at a wavelength of 374 nm as the photoionization laser of calcium atoms. The two laser beams are combined by a polarization beam splitter (PBS). To cool and repump $^{40}\text{Ca}^+$, two laser beams of wavelength 397 and 866 nm are combined by a dichromatic mirror. Two frequency-quadrupled, tunable diode laser systems (TA-FHG Pro, Toptica) are used to ionize the cadmium atoms (228 nm) and probe the $^{113}\text{Cd}^+$ (214.5 nm). The power

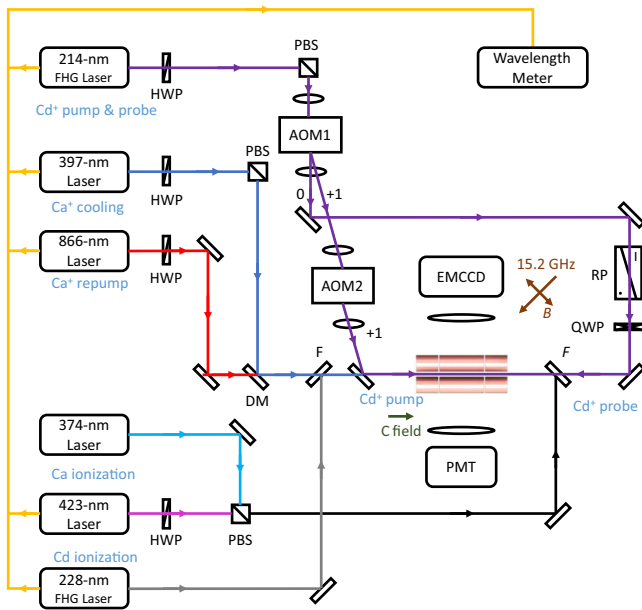


FIG. 2. Schematic of the entire experimental system. HWP, half-wave plate; QWP, quarter-wave plate; PBS, polarization beam splitter; DM, dichromatic mirror; RP, Rochon polarizer; F, mirror mounted on flipper; AOM, acousto-optic modulator; PMT, photomultiplier tube detector; EMCCD, electron-multiplying charge coupled device; other optical elements not marked are ordinary mirrors and convex lenses. Yellow arrow lines, optical fiber; dark green arrows, the direction of the C field (quantization axis); brown arrows, rf pulse (the polarization direction of the magnetic field is plotted); other arrow lines, lasers of different wavelengths (colors used are the same as in Fig. 1).

of the 228-nm laser beam is about 1 mW, whereas that of the 214.5-nm laser beam can be adjusted by a half-wave plate and another PBS. All tunable lasers are locked to a specific frequency measured by a wavelength meter (HighFinesse, WSU 8-2) via an optical fiber. Flipper optic mounts are used to ensure that the photoionizing lasers (wavelengths 374, 423, and 228 nm) can enter the vacuum chamber only during the ionizing process. A Rochon polarizer and a quarter-wave plate are used to obtain pure right-handed circularly polarized light (σ^+), ensuring a cycling transition during detection. To prepare the cadmium ion in the $^2S_{1/2} F = 0$ state (thus completing the clock transition), we use two acousto-optic modulators (AOMs) to shift the probe laser by 800 MHz for pumping. The 15.2-GHz microwave is fed into the vacuum cavity through a microwave horn. The polarization direction of the microwave magnetic field and the C-field (quantization axis) direction are at a nonorthogonal angle to ensure that both σ transitions and π transitions can be detected. The fluorescence signal from $^{113}\text{Cd}^+$ is detected by a photomultiplier tube (PMT). The ion crystal is imaged by an electron-multiplying charge-coupled device (EMCCD) to ascertain its shape and structure.

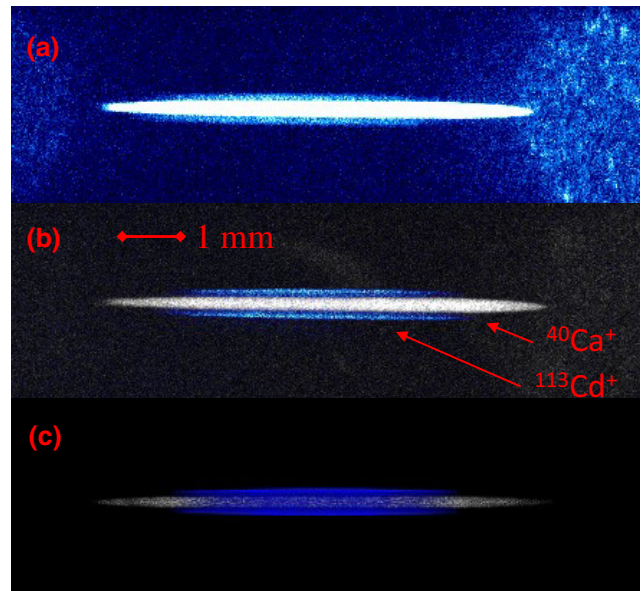


FIG. 3. Typical image of $^{40}\text{Ca}^+ - ^{113}\text{Cd}^+$ bicrystal with $V_{\text{rf}} = 170$ V $V_{\text{EC}} = 8$ V. In these pseudocolor images, $^{40}\text{Ca}^+$ ions appear white and $^{113}\text{Cd}^+$ ions appear blue. (a) Image taken by EMCCD without UV filters. Because the power of the 397-nm laser beam is much larger than that for the 214-nm beam, the fluorescence signal of $^{40}\text{Ca}^+$ is much brighter than that of $^{113}\text{Cd}^+$. Chromatic aberration prevents the two ions from showing a clear image at the same time because the wavelength difference between the two laser beams is nearly double. (b) Image synthesized from ion images under different wavelength filters, taking into account the chromatic aberration effects. (c) Molecular dynamics simulation image of the two-component ion crystal under the same conditions as for (a),(b).

The ions are confined in a linear quadrupole trap. The frequency of the rf driving voltage is 1.961 MHz, its amplitude being usually between 150 and 300 V. The EC voltage for axial confinement is about 5–10 V. To obtain sympathetically cooled ion crystals, neutral Ca atoms are first evaporated and ionized and then the ultracold $^{40}\text{Ca}^+$ crystal is obtained through Doppler cooling. Thereafter, $^{113}\text{Cd}^+$ ions are produced by ionizing evaporated atoms. By scanning the frequency of the cooling laser (397 nm) and reducing the amplitude of the rf voltage, $^{113}\text{Cd}^+$ ions are sympathetically cooled to the crystal phase [32]. A typical image of the two-component ion crystal (Fig. 3) displays an ellipsoidal $^{40}\text{Ca}^+$ crystal located in the center of the trap; the $^{113}\text{Cd}^+$ ions form a thin shell outside the $^{40}\text{Ca}^+$ crystal.

Using the zero-temperature charged-liquid model [34,35], the ion density may be estimated using the formula

$$n_i = \frac{\epsilon_0 U_{\text{rf}}^2}{M_i \Omega^2 r_0^4}, \quad (1)$$

where ϵ_0 denotes vacuum permittivity, U_{rf} the amplitude of the rf driving voltage, M_i the mass of ion, Ω the angular frequency rf driving voltage.

From the EMCCD image, the dimensions of the calcium ion crystal can be measured directly, from which the crystal volume can be estimated. However, because the cadmium ion shell is thin, deriving the volume from the EMCCD image directly results in a large uncertainty. The number of $^{113}\text{Cd}^+$ is calculated by comparing the image with that obtained from a molecular dynamics simulation [32]. In our sympathetically cooled ion frequency standard experiment, a typical value for the number of $^{40}\text{Ca}^+$ is 7500 whereas the number of $^{113}\text{Cd}^+$ is 5200.

The temperature of $^{113}\text{Cd}^+$ is a useful factor in characterizing the effect of sympathetic cooling. We evaluate the motion of the $^{113}\text{Cd}^+$ along the axis of the Paul trap, characterized by a temperature T_z , by measuring the Doppler broadening of the 214.5-nm $^{113}\text{Cd}^+$ fluorescence spectrum (Fig. 4). The measured line profiles are fitted with a Voigt curve. The Lorentz linewidth of the Voigt curve is set at 60.13 MHz, the natural linewidth of the D_2 transition of $^{113}\text{Cd}^+$ [36]. The temperature can be derived from the fitted Gaussian linewidth [37–39]

$$T_z = \frac{M_i c^2}{8 \ln 2 \times k_B} \left(\frac{v_G}{v} \right)^2, \quad (2)$$

where c denotes the speed of light in vacuum, k_B the Boltzmann constant, v_G the Gaussian linewidth, and v the resonance frequency of the D_2 transition of $^{113}\text{Cd}^+$. We can use T_z to characterize the temperature of the ion motion because the secular motion and micromotion of the ion in all directions are of the same order [40]. In

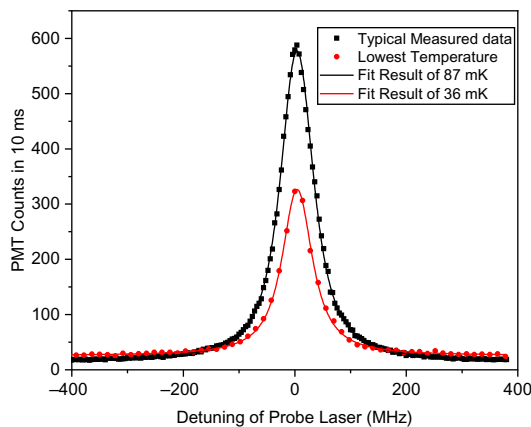


FIG. 4. Fluorescence spectra of sympathetically cooled $^{113}\text{Cd}^+$ obtained in experiments exploiting the microwave frequency standard. The black line is a fitted curve of data for measurements taken at a typical temperature of 87 mK. Similarly, the red line is a fitted curve of data for the lowest temperature reached of 36 mK.

our sympathetically cooled ion microwave frequency standard experiments, a typical Gaussian broadening is 27.6(5) MHz, corresponding to a temperature of 87(3) mK. We study the effects of different rf and EC voltages, ion ratios [32], detuning of the 397-nm laser beam, and other factors on the temperature of cadmium ions. The lowest temperature is 36(5) mK, corresponding to Gaussian linewidth of 17.8(1.3) MHz. The temperature is an order of magnitude smaller than that registered in our previous laser-cooled cadmium frequency standard (654 mK) [13].

III. CLOCK SIGNAL AND ITS STABILITY

After cooling the trapped ions, we obtain the Rabi and Ramsey fringes of the clock transition signal by microwave interrogation. Timing sequences for the Ramsey spectroscopy in the traditional laser-cooled $^{113}\text{Cd}^+$ frequency standard [13] and in the sympathetically cooled $^{113}\text{Cd}^+$ frequency standard are presented in Fig. 5. A typical Ramsey fringe is shown in Fig. 6. To see the shape of Ramsey fringes clearly, the free evolution time is chosen to be 500 ms instead of 5000 ms as noted in Fig. 5(b).

During the sympathetic cooling period of the timing sequence, we measure the loss rate of ions [32]. The lifetime of $^{40}\text{Ca}^+$ is measured from the 397-nm fluorescence decay and is estimated to be more than one day. As for $^{113}\text{Cd}^+$, we measure the signal strength at half-height of the Ramsey fringe decay, which falls off exponentially. The lifetime ($1/e$) is estimated to be up to about 2×10^4 s, 3 times longer than that in a typical laser-cooling scheme [13].

Compared with traditional laser-cooled ion frequency standards, the sympathetically cooled ion frequency standard removes laser cooling process from the timing sequence. The dead time per loop (for Ramsey method) is reduced from 870 to 370 ms so that the Dick effect that appears because of the dead time is suppressed.

Moreover, sympathetic cooling can ensure that the cadmium ions are not heated by the rf during microwave interrogation. The SODFS caused by the thermal motion

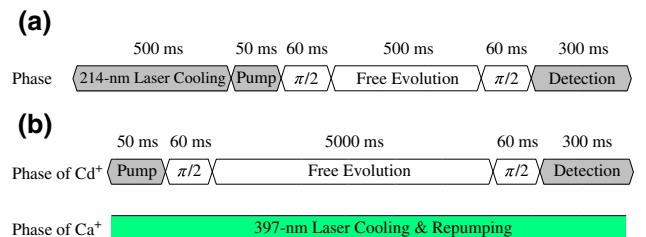


FIG. 5. Timing sequences for Ramsey's separated oscillatory field method for (a) a traditional laser-cooled $^{113}\text{Cd}^+$ frequency standard [13] and (b) a sympathetically cooled $^{113}\text{Cd}^+$ frequency standard. Dead time is marked with a gray background. A 20-ms duration waiting for a circuit response is not shown in the figure.

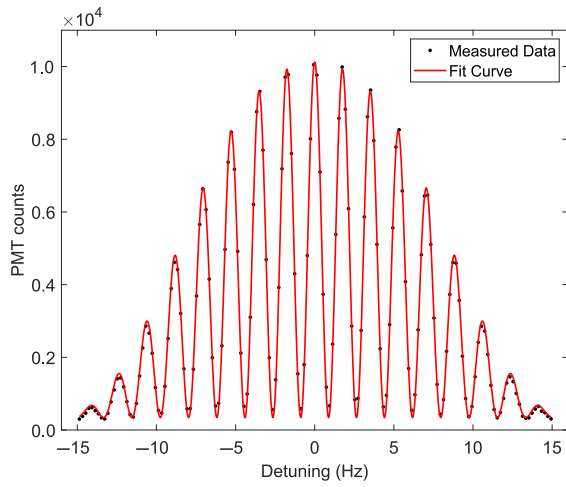


FIG. 6. Typical high signal-to-noise ratio Ramsey fringe obtained from our sympathetically cooled ion frequency standard operating at a clock transition of 15.2 GHz with a free evolution time of 500 ms, two phase-coherent microwave pulses of 60 ms, and a fluorescence signal integration time of 300 ms.

of ions is effectively suppressed in the sympathetic cooling scheme thereby allowing the free evolution time to be extended. The frequency stability of a frequency standard is characterized by the Allan deviation and its theoretical limit is obtained from [39]

$$\sigma_y(\tau) = \frac{1}{K_0} \frac{1}{Q} \frac{1}{\text{SNR}} \sqrt{\frac{T_c}{\tau}}, \quad (3)$$

for which K_0 is a constant of order unity and $K_0 = \pi$ for the Ramsey case; Q is the quality factor $Q = \nu_0/\Delta\nu$, where ν_0 is the clock transition frequency and $\Delta\nu$ is the full width at half maximum of the Ramsey peak; SNR denotes the signal-to-noise ratio, T_c the total cycle time, and τ the averaging time of stability. In Eq. (3), Q and T_c are related to the free evolution time T_f , specifically, $Q = \nu_0/\Delta\nu = 2T_f\nu_0$ and $T_c = T_f + T_d + 2T_p$. In our experiments, dead time is $T_d = 370$ ms, and the duration of the $\pi/2$ pulse is $T_p = 60$ ms. When the free evolution time is much longer than either the dead time or the pulse time, the ultimate frequency stability σ_y follows that $\sqrt{T_c/Q} = 1/2\nu_0 1/\sqrt{T_f}$ dependence given the same SNR. Therefore, extending the free evolution time is beneficial in reducing the theoretical limit of the Allan deviation.

However, as the free evolution time increases, the peak-to-peak value of the Ramsey fringes decreases because of decoherence in the $^{113}\text{Cd}^+$ crystal. Noise also increases because of magnetic field fluctuations and ion collisions, among other factors. The reduction of the SNR limits the extension of the free evolution time. To obtain a suitable free evolution time, we measure the coherence lifetime of sympathetically cooled $^{113}\text{Cd}^+$ (Fig. 7). We first measure the PMT counts of the amplitude of Ramsey fringes

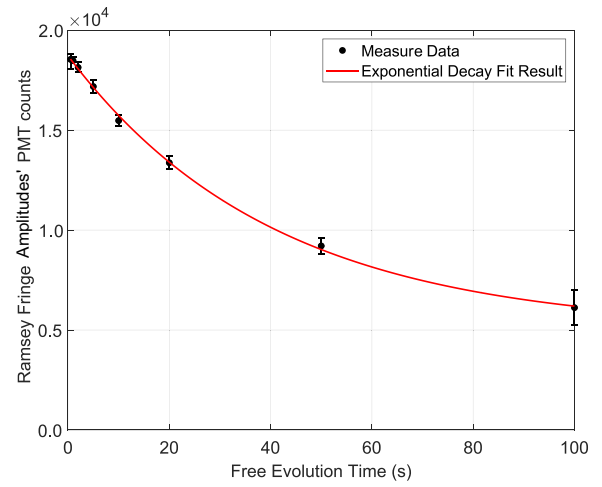


FIG. 7. Measurement of Ramsey fringe amplitudes corresponding to different free evolution times. The amplitude is calculated from a cosine fit to the central peak of the Ramsey fringe.

at short free evolution time and then gradually increase the free evolution time, observing the decay of the amplitude. The exponential decay fitting gives a $1/e$ lifetime of 41 s. Taking into account ion loss (the $1/e$ lifetime of trapped $^{113}\text{Cd}^+$ 2×10^4 s) in long-term measurements (one and a half hours' measurement for the same ion ensemble) also results in a reduction in amplitude of Ramsey fringes, the coherence lifetime should be slightly longer than the 41-s duration obtained by fitting. Taking the above factors into consideration, the free evolution time of closed-loop locking is set at 5 s.

The local oscillator (LO) of the frequency standard is an oven controlled crystal oscillator (OCXO) with a frequency stability of 2×10^{-13} at 1 s (Fig. 8, red line). A microwave synthesizer (8257D, Agilent) converts the LO's 10-MHz signal to 15.2 GHz. By frequency hopping at the left and right half-heights of the central peak ($\nu_0 \pm \Delta\nu/2$), the error signal is obtained by taking the difference between the left and right signal strengths. The error signal is fed to a digital proportional-integral-differentiation (PID) controller to generate a feedback voltage to the LO. Once the LO is controlled by the $^{113}\text{Cd}^+$, its output of 10 MHz is fed to a phase noise analyzer (5120A, Symmetricom) referenced to a hydrogen maser (MHM 2010, Microsemi) for characterization.

The stability measurement of closed-loop locking is marked as a solid blue line in Fig. 8. The free evolution time of Ramsey's separated oscillatory fields is 5 s and the feedback loop time is 11 s due to frequency hopping. The Allan deviation for times shorter than the loop time is determined using the LO whereas that for longer than the loop time is determined by the ions, indicating a short-term frequency stability of $3.48 \times 10^{-13}/\sqrt{\tau}$. The

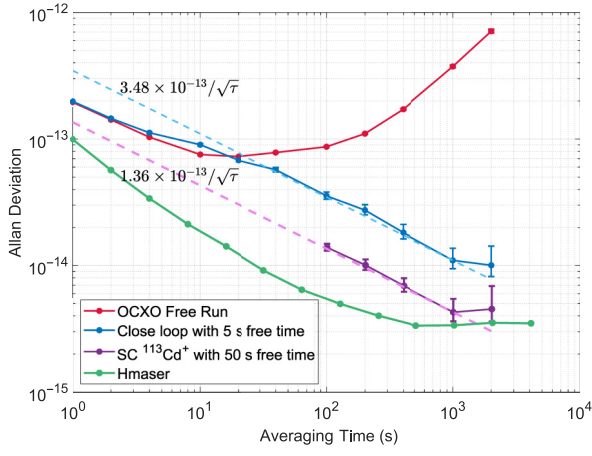


FIG. 8. Allan deviations of the sympathetically cooled $^{113}\text{Cd}^+$ microwave frequency standard. The solid red line is the stability of the free-running OCXO measured by a phase noise analyzer. The solid blue line is the stability of the OCXO locked on the Ramsey fringe of sympathetically cooled $^{113}\text{Cd}^+$ with a free evolution time of 5 s, measured by the phase noise analyzer. The purple solid line is the stability derived from the Ramsey fringe error signal obtained from frequency-hopping measurements. The light blue and purple dashed lines are the $\tau^{-1/2}$ fits of the solid lines. The green solid line is the fractional frequency stability of the hydrogen maser (MHM 2010) used in our laboratory.

measurement lasted for 5 h (18 047 s) and the Allan deviation at 2000 s is 1.01×10^{-14} . Longer measurement times and larger averaging time τ did not result in better stability, possibly because of a reduced SNR and frequency drift from ion loss.

The short-term frequency stability seems not to have improved much compared with previous results from the laser-cooling scheme ($4.2 \times 10^{-13}/\sqrt{\tau}$ in Ref. [13]). The main reason is that the previous results [11–13] characterized the stability using a modified Allan deviation, which occurs usually in the presence of fast noise processes [41,42], such as those produced by ultrastable lasers rather than atomic clocks. For white frequency noise ($\sigma_y \propto \tau^{-1/2}$), Allan deviation is $\sqrt{2}$ times the modified Allan deviation.

To evaluate the limit of short-term stability, we need to consider the Dick effect and the influence of various types of noise. We measure the phase noise power spectral density of our LO at 15.2 GHz via a phase noise analyzer (53100A, Microchip). Bringing in the experimental parameters of our closed-loop measurements, we obtain an Allan deviation for the Dick effect contribution of $3.5 \times 10^{-14}/\sqrt{\tau}$, one-tenth that for laser-cooling scheme ($3.43 \times 10^{-13}/\sqrt{\tau}$ in Ref. [13]).

Considering the contribution of SNR to short-term stability, we characterize the signal strength by half the peak-to-peak value of PMT counts of the central Ramsey

fringe. For a multi-ion frequency standard, the system noise of PMT counts, including quantum projection noise, shot noise, and pump noise [43], can be calculated from the Ramsey fringes and the number of ions:

$$\begin{aligned}\sigma_{\text{proj}} &= \frac{1}{2}K\sqrt{\eta N}, \\ \sigma_{\text{shot}} &= \sqrt{\frac{S+s}{2}}, \\ \sigma_{\text{pump}} &= \frac{\sqrt{N\eta(1-\eta)}K}{2},\end{aligned}\quad (4)$$

where S denotes the maximum counts of Ramsey fringes, s the minimum counts of Ramsey fringes, N the number of the $^{113}\text{Cd}^+$, K the number of photons stimulated radiated per ion with $K = (S - B)/N$, B the PMT background counts without ions, and η the pump efficiency with $\eta = 1 - (s - B)/(S - B)$. The contribution of quantum projection noise, shot noise, and pump noise to the Allan deviation are $1.06 \times 10^{-13}/\sqrt{\tau}$, $7.7 \times 10^{-14}/\sqrt{\tau}$, and $4.4 \times 10^{-14}/\sqrt{\tau}$, respectively. Summing the squares of each noise gives the total system noise, which contributes $1.38 \times 10^{-13}/\sqrt{\tau}$ to the Allan deviation. The rest of the Allan deviation comes from technical noise, including fluctuations in laser frequency and power, temperature fluctuations, and circuit noise during the PID process.

To explore the limit of short-term frequency stability, we extend the free evolution time to its extreme of 50 s. Over this period, the instability of the LO has a substantial influence, and hence we adopt an indirect measurement method. We use the hydrogen maser (MHM 2010) as a LO, and calculate the relative frequency difference through the error signal, thereby obtaining the Allan deviation indirectly. The 1.6×10^4 s measurement is marked as a purple dashed line in Fig. 8. The short-term frequency stability of the measurement is $1.36 \times 10^{-13}/\sqrt{\tau}$. For comparison, the fractional frequency stability of the hydrogen maser is also shown as the green line in Fig. 8. There is still room for improvement in our sympathetically cooled ion frequency standard.

IV. UNCERTAINTY EVALUATIONS

We first discuss the second-order Zeeman frequency shift (SOZFS), which is the main source of systematic uncertainty in this work. We measure the Rabi fringe of the magnetic-field-sensitive transition ($|F = 0, m_F = 0\rangle \rightarrow |F' = 1, m'_F = \pm 1\rangle$, Fig. 9), and the SOZFS, the fractional values of which are given by

$$\begin{aligned}\frac{\delta\nu_{\text{SOZFS}}}{\nu_0} &= \frac{(g_J - g_I)^2 \mu_B^2}{2h^2\nu_0^2} B^2 \\ &= \frac{1}{2\nu_0^2} \left(\frac{g_J - g_I}{g_J + g_I} \right)^2 \times (\nu_{0-1} - \nu_{0+1})^2,\end{aligned}\quad (5)$$

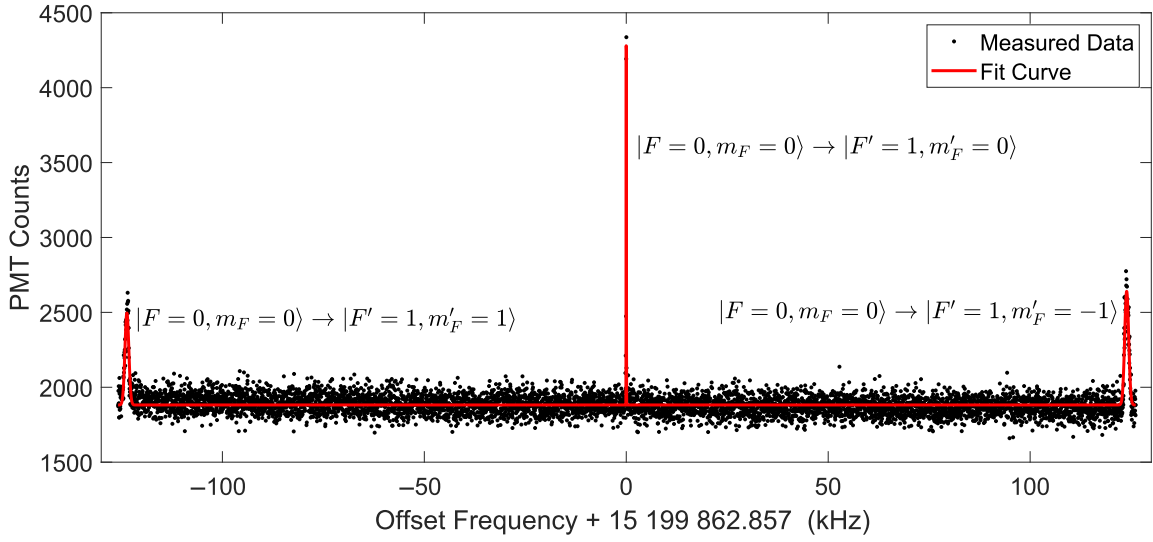


FIG. 9. Rabi fringe of the ground-state hyperfine transition ($|F = 0, m_F = 0\rangle \rightarrow |F' = 1, m'_F = 0, \pm 1\rangle$). The three peaks from left to right correspond to the $m_F = 0 \rightarrow 1$, $m_F = 0 \rightarrow 0$, and $m_F = 0 \rightarrow -1$ transition, respectively. The power of the 15.2 GHz π pulse is -9 dBm; a range of 25.2 kHz is scanned in steps of 40 Hz.

where ν_0 denotes the ground-state hyperfine splitting of $^{113}\text{Cd}^+$, μ_B Bohr magneton, h Planck constant, g_J and g_I denote the respective Landé g -factors of the electron and the nucleus, having values $g_J = 2.002\,291(4)$ [44] and $g_I = 0.622\,300\,9(9) \times 10^{-3}$ [45], and ν_{0-1} and ν_{0+1} denote the frequencies of magnetic-field-sensitive transition we measured. The frequency difference between the two peaks of the magnetic-field-sensitive transition is 247 488(10) Hz, and hence the magnetic field strength is 8828.3(4) nT with a fractional SOZFS of $1.32\,391(11) \times 10^{-10}$. The calculated result is larger than that presented in Ref. [31] because the C field in the experiment is larger than the ideal case.

Before calculating the SODFS, we should analyze in advance the contributions to the ion velocity of the different motions. The motion of ions in a Paul trap can be decomposed into secular motion, micromotion induced by the rf field, and the excess micromotion induced by the phase difference between the two rf electrodes or additional electrostatic fields [40]. For the first two, their contributions to SODFS can be calculated using [46]

$$\frac{\delta\nu_{\text{SODFS-s\&m}}}{\nu_0} = -\frac{3k_B T}{2Mc^2} \left(1 + \frac{2}{3}N_d^K\right), \quad (6)$$

where T denotes the temperature of the ion ensemble [here, we can use 87(3) mK obtained in Sec. 2], and $N_d^K = 3$ set the SODFS coefficient associated with the micromotion. The fractional SODFS is calculated to be $-3.21(11) \times 10^{-16}$. However, for sympathetically cooled large-size ion crystals in a linear Paul trap, excess micromotion provides the dominant contribution to the SODFS. We can suppose the interaction of calcium ions with cadmium ions as a constant electrostatic field, forcing the cadmium

ions to deviate from the central axis of the Paul trap. Its contribution to the SODFS may be calculated from

$$\frac{\delta\nu_{\text{SODFS-ex}}}{\nu_0} = -\frac{1}{16} \frac{q^2 \Omega^2 u^2}{c^2}, \quad (7)$$

where q denotes a dimensionless quantity describing the motion of the ion with $q = 2Q_i U_{\text{rf}} / (M_i \Omega^2 r_0^2)$, Q_i and M_i denote the charge and mass of $^{113}\text{Cd}^+$, and u denotes the distance of the ion from the central axis of the Paul trap. This distance can be estimated from the ion crystal size using the EMCCD images; hence, the fractional SODFS contributed by excess micromotion is calculated to be $-2.4(3) \times 10^{-14}$. The SODFS contributed by the excess micromotion also limits the number of trapped ions. We cannot blindly increase the number of $^{113}\text{Cd}^+$ to improve the SNR, because that will increase the SODFS at the same time.

We discuss the Stark frequency shift separately depending on the source. Because all of the 214.5-nm laser beams are blocked by mechanical shutters during the microwave interrogation, its contribution to light frequency shifts is negligible. However, because both cooling and repump lasers remain on during the microwave interrogation, the sympathetic cooling scheme will introduce additional light frequency shifts [31] compared with those from laser cooling. Substituting in the light intensity for our experiment (which is the same as that described in Ref. [31]), the number of $^{40}\text{Ca}^+$ (7500), and the surface area of the calcium ion crystals (6.9 mm^2), we obtain the light frequency shifts contributed by the laser beams and the fluorescence being $5.4(5) \times 10^{-17}$ and $1.2(1.2) \times 10^{-21}$, respectively.

The Stark shifts generated by the electric field of the ion trap, may be estimated from the average of the square of the ion velocities $\langle V^2 \rangle$ [40], which may be calculated from the SODFS, specifically $\delta\nu_{\text{SODFS}}/\nu_0 = -\langle V^2 \rangle/(2c^2)$, and given by

$$\frac{\delta\nu_{\text{S-trap}}}{\nu_0} = \frac{\sigma_S}{\nu_0} \left(\frac{m\Omega}{Q_i} \right)^2 \langle V^2 \rangle, \quad (8)$$

where σ_S denotes the static Stark shift coefficient and is calculated to be $3.99(11) \times 10^{-12}$ Hz/(V/m)² [47]. Therefore, the Stark frequency shifts contributed by the ac quadrupole electric field (corresponding to the secular motion and micromotion) and the electrostatic field generated by the calcium ions (corresponding to the excess micromotion) are $3.14(14) \times 10^{-18}$ and $2.3(3) \times 10^{-16}$, respectively.

The Stark frequency shift from the blackbody radiation contribution (BBRS) can be obtained from Ref. [47]. The room temperature is about 300 K; considering the room-temperature fluctuations and the effect of rf heating on the temperature of the trap electrodes [48], the effective temperature fluctuation of the blackbody radiation incident on the ion should be no more than 10 K. The fractional BBRS shift and its uncertainty is $-1.8(2) \times 10^{-16}$. Similarly, the Zeeman frequency shift of the blackbody radiation (BBRZ) along with its uncertainty is calculated to be $-9.8(7) \times 10^{-18}$ [49].

For the ac Zeeman shift contributed by the quadrupole field, the ac magnetic field vanishes if the trap structure is physically and electrically symmetric [50]. In estimating its uncertainty, we can give an upper bound to the ac magnetic field of 10^{-10} T obtained from the electric field average [40] and the rf frequency, which contributes an ac Zeeman shift less than 2×10^{-20} .

The gravitational redshift has a magnitude of 1.1×10^{-16} per meter of the change in height at sea level [51].

The altitude of the experimental system in our laboratory is 43 ± 1 m [13] so that the fractional frequency shift resulting from the gravitational redshift is estimated to be $4.73(11) \times 10^{-15}$ compared to sea level.

For laser-cooled ions, the pressure frequency shift is negligible for an ultrahigh vacuum (and the same situation for sympathetic cooling cases). Assuming the pressure shift coefficient for $^{113}\text{Cd}^+$ is of the same order as for $^{171}\text{Yb}^+$ [52] and $^{199}\text{Hg}^+$ [53], and considering the pressure in the vacuum chamber is below 1×10^{-9} Pa and mostly contributed by He and H₂, the uncertainty in the pressure frequency shift is no more than 10^{-17} .

From the systematic frequency shifts and corresponding uncertainties listed in Table I, the SOZFS contributes most of the uncertainty and is larger than previous results [13]. Although the strength of the C field in this work is similar to that in the previous work [13], its uncertainty is larger in this work, probably because the magnetic shield barrel deteriorates from long-term use or the vacuum chamber and some stainless steel segments in the chamber are magnetized, causing a magnetic field gradient. Outside magnetic fluctuations during the experiment may also result in a larger uncertainty of magnetic field in measurement. The good news is that the SODFS is half smaller than that of the laser cooling scheme, and the additional light frequency shift introduced by sympathetic cooling can be ignored. Taking into account the type A uncertainty ($\sigma_y = 1.01 \times 10^{-14}$ @ 2000 s), the total uncertainty for the sympathetically cooled $^{113}\text{Cd}^+$ frequency standard is 1.5×10^{-14} , which is superior to the level obtained from laser-cooled cadmium ions frequency standard (1.8×10^{-14} in Ref. [13]).

V. CONCLUSIONS AND DISCUSSIONS

We build a high-performance Paul-trap-based sympathetically cooled ion microwave frequency standard, based

TABLE I. Estimation of systematic frequency shifts and uncertainties.

Shift	Fractional magnitude of effect		Fractional uncertainties	
SOZFS	1.32 391	$\times 10^{-10}$	1.1	$\times 10^{-14}$
SODFS by secular and micro- motion	-3.21	$\times 10^{-16}$	1.1	$\times 10^{-17}$
SODFS by excess micromotion	-2.4	$\times 10^{-14}$	3	$\times 10^{-15}$
light shift by 214.5 nm	0		0	
light shift by 397 & 866 nm (laser)	5.4	$\times 10^{-17}$	5	$\times 10^{-18}$
light shift by 397 & 866 nm (flou.)	1.2	$\times 10^{-21}$	1.2	$\times 10^{-21}$
ac Stark by quadrupole field	3.14	$\times 10^{-18}$	1.4	$\times 10^{-19}$
dc Stark by Ca ⁺ electrostatic field	2.3	$\times 10^{-16}$	3	$\times 10^{-17}$
BBRS	-1.8	$\times 10^{-16}$	2	$\times 10^{-17}$
BBRZ	-9.8	$\times 10^{-18}$	7	$\times 10^{-19}$
ac Zeeman by quadrupole field	0		<2	$\times 10^{-20}$
gravitational red shift	4.73	$\times 10^{-15}$	1.1	$\times 10^{-16}$
pressure shift	0		<1	$\times 10^{-17}$
Total	1.32 371	$\times 10^{-10}$	1.1	$\times 10^{-14}$

on $^{113}\text{Cd}^+$ ions cooled by coolant ions of laser-cooled $^{40}\text{Ca}^+$. Sympathetically cooled cadmium ions can attain ultralow temperatures of 36 mK with coherent lifetimes exceeding 40 s. In adopting the sympathetic cooling method, the dead time can be compressed from 870 to 370 ms, and the free evolution time of the closed loop can be extended from 0.5 to 5 s so that the Dick effect is suppressed to one-tenth that of the laser-cooling scheme (from $3.43 \times 10^{-13}/\sqrt{\tau}$ in Ref. [13] to $3.5 \times 10^{-14}/\sqrt{\tau}$ in this study). We achieve a closed-loop locking experiment with a short-term frequency stability of $3.48 \times 10^{-13}/\sqrt{\tau}$, close to the level of the laser-cooled mercury ions' microwave clock ($3.3 \times 10^{-13}/\sqrt{\tau}$ in Ref. [10]), although the $^{113}\text{Cd}^+$ clock's transition frequency (15.2 GHz) is about 1/3 that of $^{199}\text{Hg}^+$ (40.5 GHz). The fractional uncertainty is 1.5×10^{-14} , better than that for laser-cooled cadmium ions' frequency standard (1.8×10^{-14} in Ref. [13]). The improvement in accuracy is mainly because of the reductions in type A uncertainties and SODFS uncertainties. In exploring the limits of sympathetically cooled ion microwave frequency standard, the stability of the 50-s free evolution is measured indirectly to be $1.36 \times 10^{-13}/\sqrt{\tau}$ with a hydrogen maser as LO.

In the future, we will focus on the long-term frequency stability of the sympathetically cooled ion microwave frequency standard, as it is an essential part of the performance of microwave frequency standards and reducing the type A uncertainty can give higher frequency accuracy. Moreover, $^{174}\text{Yb}^+$ is seen as a replacement for $^{40}\text{Ca}^+$ in experiments to attain higher performance [54]. Miniaturization is also another consideration because the sympathetically cooled ion microwave frequency standard holds promise in establishing a ground-based time frequency reference for future satellite navigation systems.

ACKNOWLEDGMENTS

The authors thank Dr. Zheng-Bo Wang, Dr. Kai Miao, Dr. Chen-Fei Wu, Dr. Ya-ni Zuo, Li-Ming Guo, Hua-Xing Hu, Wen-Xin Shi, Tian-Gang Zhao, and Ying Zheng for helpful assistance and discussions. This work is supported by National Key Research and Development Program of China (2016YFA0302100, 2021YFA1402101), and National Natural Science Foundation of China (12073015).

-
- [1] T. Bandi, C. Affolderbach, C. E. Calosso, and G. Miletì, High-performance laser-pumped rubidium frequency standard for satellite navigation, *Electron. Lett.* **47**, 698 (2011).
 - [2] L. A. Mallette, J. White, and P. Rochat, in *Proceedings of IEEE/ION Position, Location and Navigation Symposium* (IEEE, Indian Wells, CA, USA, 2010), p. 903.
 - [3] J. Ho, I. Pascaru, C. Stone, and T. McClelland, in *Proceedings of the 1998 IEEE International Frequency Control Symposium (Cat. No. 98CH36165)* (IEEE, Pasadena, CA, USA, 1998), p. 80.

- [4] S. A. Diddams, J. C. Bergquist, S. R. Jefferts, and C. W. Oates, Standards of time and frequency at the outset of the 21st century, *Science* **306**, 1318 (2004).
- [5] E. A. Burt, W. A. Diener, and R. L. Tjoelker, A compensated multi-pole linear ion trap mercury frequency standard for ultra-stable timekeeping, *IEEE Trans. Ultrason. Ferroelectr. Freq. Control* **55**, 2586 (2008).
- [6] E. Burt, J. Prestage, R. Tjoelker, D. Enzer, D. Kuang, D. Murphy, D. Robison, J. Seubert, R. Wang, and T. Ely, Demonstration of a trapped-ion atomic clock in space, *Nature* **595**, 43 (2021).
- [7] L. Liu, D.-S. Lü, W.-B. Chen, T. Li, Q.-Z. Qu, B. Wang, L. Li, W. Ren, Z.-R. Dong, J.-B. Zhao *et al.*, In-orbit operation of an atomic clock based on laser-cooled 87 Rb atoms, *Nat. Commun.* **9**, 1 (2018).
- [8] J. D. Prestage and G. L. Weaver, Atomic clocks and oscillators for deep-space navigation and radio science, *Proc. IEEE* **95**, 2235 (2007).
- [9] J. D. Prestage, G. Dick, and L. Maleki, in *44th Annual Symposium on Frequency Control* (IEEE, Baltimore, MD, USA, 1990), p. 82.
- [10] D. J. Berkeley, J. D. Miller, J. C. Bergquist, W. M. Itano, and D. J. Wineland, Laser-Cooled Mercury Ion Frequency Standard, *Phys. Rev. Lett.* **80**, 2089 (1998).
- [11] J. Zhang, S. Wang, K. Miao, Z. Wang, and L. Wang, Toward a transportable microwave frequency standard based on laser-cooled $^{113}\text{Cd}^+$ ions, *Appl. Phys. B* **114**, 183 (2014).
- [12] K. Miao, J. W. Zhang, X. L. Sun, S. G. Wang, A. M. Zhang, K. Liang, and L. J. Wang, High accuracy measurement of the ground-state hyperfine splitting in a $^{113}\text{Cd}^+$ microwave clock, *Opt. Lett.* **40**, 4249 (2015).
- [13] S. N. Miao, J. W. Zhang, H. R. Qin, N. C. Xin, J. Z. Han, and L. J. Wang, Precision determination of the ground-state hyperfine splitting of trapped $^{113}\text{Cd}^+$ ions, *Opt. Lett.* **46**, 5882 (2021).
- [14] P. Phoonthong, M. Mizuno, K. Kido, and N. Shiga, Determination of the absolute microwave frequency of laser-cooled $^{171}\text{Yb}^+$, *Appl. Phys. B* **117**, 673 (2014).
- [15] S. Mulholland, H. Klein, G. Barwood, S. Donnellan, P. Nisbet-Jones, G. Huang, G. Walsh, P. Baird, and P. Gill, Compact laser system for a laser-cooled ytterbium ion microwave frequency standard, *Rev. Sci. Instrum.* **90**, 033105 (2019).
- [16] N. C. Xin, H. R. Qin, S. N. Miao, Y. T. Chen, Y. Zheng, J. Z. Han, J. W. Zhang, and L. J. Wang, Laser-cooled $^{171}\text{Yb}^+$ microwave frequency standard with a short-term frequency instability of $8.5 \times 10^{-13}/\sqrt{\tau}$, *Opt. Express* **30**, 14574 (2022).
- [17] T. W. Hänsch and A. L. Schawlow, Cooling of gases by laser radiation, *Opt. Commun.* **13**, 68 (1975).
- [18] A. Ashkin, Trapping of Atoms by Resonance Radiation Pressure, *Phys. Rev. Lett.* **40**, 729 (1978).
- [19] D. J. Wineland, R. E. Drullinger, and F. L. Walls, Radiation-Pressure Cooling of Bound Resonant Absorbers, *Phys. Rev. Lett.* **40**, 1639 (1978).
- [20] W. Neuhauser, M. Hohenstatt, P. Toschek, and H. Dehmelt, Optical-Sideband Cooling of Visible Atom Cloud Confined in Parabolic Well, *Phys. Rev. Lett.* **41**, 233 (1978).

- [21] S.-Y. Dai, F.-S. Zheng, K. Liu, W.-L. Chen, Y.-G. Lin, T.-C. Li, and F. Fang, Cold atom clocks and their applications in precision measurements, *Chin. Phys. B* **30**, 013701 (2021).
- [22] G. Panfilo and F. Arias, The coordinated universal time (UTC), *Metrologia* **56**, 042001 (2019).
- [23] S. Bize, The unit of time: Present and future directions, *C. R. Phys.* **20**, 153 (2019).
- [24] S. M. Brewer, J.-S. Chen, A. M. Hankin, E. R. Clements, C.-w. Chou, D. J. Wineland, D. B. Hume, and D. R. Leibbrandt, $^{27}\text{Al}^+$ Quantum-Logic Clock with a Systematic Uncertainty Below 10^{-18} , *Phys. Rev. Lett.* **123**, 033201 (2019).
- [25] S. Hannig, L. Pelzer, N. Scharnhorst, J. Kramer, M. Stepanova, Z. Xu, N. Spethmann, I. Leroux, T. Mehlstäubler, and P. Schmidt, Towards a transportable aluminium ion quantum logic optical clock, *Rev. Sci. Instrum.* **90**, 053204 (2019).
- [26] Z. Y. Ma, H. L. Liu, W. Z. Wei, W. H. Yuan, P. Hao, Z. Deng, H. Che, Z. T. Xu, F. H. Cheng, Z. Y. Wang, K. Deng, J. Zhang, and Z. H. Lu, Investigation of experimental issues concerning successful operation of quantum-logic-based $^{27}\text{Al}^+$ ion optical clock, *Appl. Phys. B* **126**, 1 (2020).
- [27] S.-J. Chao, K.-F. Cui, S.-M. Wang, J. Cao, H.-L. Shu, and X.-R. Huang, Observation of $^1S_0 \rightarrow ^3P_0$ transition of a $^{40}\text{Ca}^+ - ^{27}\text{Al}^+$ quantum logic clock, *Chin. Phys. Lett.* **36**, 120601 (2019).
- [28] J. Bollinger and J. Heinzen, A 303-MHz frequency standard based on trapped, *IEEE Trans. Instrum. Meas.* **40**, 126 (1991).
- [29] B. J. McMahon and B. C. Sawyer, Second-Scale $^9\text{Be}^+$ Spin Coherence in a Compact Penning Trap, *Phys. Rev. Appl.* **17**, 014005 (2022).
- [30] Y. N. Zuo, J. Z. Han, J. W. Zhang, and L. J. Wang, Direct temperature determination of a sympathetically cooled large $^{113}\text{Cd}^+$ ion crystal for a microwave clock, *Appl. Phys. Lett.* **115**, 061103 (2019).
- [31] J. Z. Han, H. R. Qin, N. C. Xin, Y. M. Yu, V. A. Dzuba, J. W. Zhang, and L. J. Wang, Toward a high-performance transportable microwave frequency standard based on sympathetically cooled $^{113}\text{Cd}^+$ ions, *Appl. Phys. Lett.* **118**, 101103 (2021).
- [32] S. N. Miao, H. R. Qin, N. C. Xin, Y. T. Chen, J. W. Zhang, and L. J. Wang, Sympathetic cooling of a large $^{113}\text{Cd}^+$ ion crystal with $^{40}\text{Ca}^+$ in a linear paul trap, [arXiv:2201.03377](https://arxiv.org/abs/2201.03377) [physics.atom-ph] (2022).
- [33] D. Denison, Operating parameters of a quadrupole in a grounded cylindrical housing, *J. Vac. Sci. Technol.* **8**, 266 (1971).
- [34] D. Wineland, in *Proceedings of the Cooling, Condensation, and Storage of Hydrogen Cluster Ions Workshop*, Menlo Park (Menlo Park, CA, USA, 1987), p. 181.
- [35] L. Hornekær, N. Kjærgaard, A. M. Thommesen, and M. Drewsen, Structural Properties of Two-Component Coulomb Crystals in Linear Paul Traps, *Phys. Rev. Lett.* **86**, 1994 (2001).
- [36] D. L. Moehring, B. B. Blinov, D. W. Gidley, R. N. Kohn Jr, M. J. Madsen, T. D. Sanderson, R. S. Vallery, and C. Monroe, Precision lifetime measurements of a single trapped ion with ultrafast laser pulses, *Phys. Rev. A* **73**, 023413 (2006).
- [37] M. Drewsen, L. Hornekær, N. Kjærgaard, K. Mølhave, A. M. Thommesen, Z. Videsen, A. Mortensen, and F. Jensen, in *AIP Conference Proceedings*, (American Institute of Physics, San Diego, California, 2002), Vol. 606, p. 135.
- [38] R. B. Warrington, P. T. Fisk, M. J. Wouters, and M. A. Lawn, Temperature of laser-cooled $^{171}\text{Yb}^+$ ions and application to a microwave frequency standard, *IEEE Trans. Ultrason. Ferroelectr. Freq. Control* **49**, 1166 (2002).
- [39] F. Riehle, *Frequency Standards: Basics and Applications* (John Wiley & Sons, Weinheim, Germany, 2006).
- [40] D. J. Berkeland, J. D. Miller, J. C. Bergquist, W. M. Itano, and D. J. Wineland, Minimization of ion micromotion in a Paul trap, *J. Appl. Phys.* **83**, 5025 (1998).
- [41] E. Rubiola, *Phase Noise and Frequency Stability in Oscillators* (Cambridge University Press, Cambridge, UK, 2008).
- [42] W. J. Riley, *Handbook of Frequency Stability Analysis* (US Department of Commerce, National Institute of Standards and Technology, Boulder, CO, USA, 2008).
- [43] W. M. Itano, J. C. Bergquist, J. J. Bollinger, J. M. Gilligan, D. J. Heinzen, F. L. Moore, M. G. Raizen, and D. J. Wineland, Quantum projection noise: Population fluctuations in two-level systems, *Phys. Rev. A* **47**, 3554 (1993).
- [44] Y. M. Yu, B. K. Sahoo, and B. B. Suo, Ground-state g_J factors of the Cd^+ , Yb^+ , and Hg^+ ions, *Phys. Rev. A* **102**, 062824 (2020).
- [45] P. Spence and M. McDermott, Optical orientation of $6.7\text{h}^{107}\text{Cd}$, *Phys. Lett. A* **42**, 273 (1972).
- [46] J. D. Prestage, R. L. Tjoelker, and L. Maleki, in *Proceedings of the 1999 Joint Meeting of the European Frequency and Time Forum and the IEEE International Frequency Control Symposium (Cat. No. 99CH36313)*, (IEEE, Besancon, France, 1999), Vol. 1, p. 121.
- [47] Y. M. Yu and B. K. Sahoo, Estimation of the blackbody-radiation shift due to the Stark effect for the microwave $^{113}\text{Cd}^+$ ion clock, *Phys. Rev. A* **96**, 050502(R) (2017).
- [48] M. Doležal, P. Balling, P. B. Nisbet-Jones, S. A. King, J. M. Jones, H. A. Klein, P. Gill, T. Lindvall, A. E. Wallin, M. Merimaa, C. Tamm, C. Sanner, N. Huntemann, N. Scharnhorst, I. D. Leroux, P. O. Schmidt, T. Burgermeister, T. E. Mehlstäubler, and E. Peik, Analysis of thermal radiation in ion traps for optical frequency standards, *Metrologia* **52**, 842 (2015).
- [49] J. Han, Y. Zuo, J. Zhang, and L. Wang, Theoretical investigation of the black-body Zeeman shift for microwave atomic clocks, *Eur. Phys. J. D* **73**, 1 (2019).
- [50] W. H. Oskay, S. A. Diddams, E. A. Donley, T. M. Fortier, T. P. Heavner, L. Hollberg, W. M. Itano, S. R. Jefferts, M. J. Delaney, K. Kim, F. Levi, T. E. Parker, and J. C. Bergquist, Single-Atom Optical Clock with High Accuracy, *Phys. Rev. Lett.* **97**, 020801 (2006).
- [51] C.-W. Chou, D. B. Hume, T. Rosenband, and D. J. Wineland, Optical clocks and relativity, *Science* **329**, 1630 (2010).
- [52] S. Park, P. Manson, M. Wouters, R. Warrington, M. Lawn, and P. Fisk, in *2007 IEEE International Frequency Control Symposium Joint with the 21st European Frequency and Time Forum* (IEEE, Geneva, Switzerland, 2007), p. 613.

- [53] S. K. Chung, J. D. Prestage, R. L. Tjoelker, and L. Maleki, in *Proceedings of the 2004 IEEE International Frequency Control Symposium and Exposition, 2004*. (IEEE, Montreal, QC, Canada, 2004), p. 130.
- [54] S. Miao, J. Zhang, N. Xin, L. Guo, H. Hu, W. Shi, H. Qin, J. Han, and L. Wang, in *2021 Joint Conference of the European Frequency and Time Forum and IEEE International Frequency Control Symposium (EFTF/IFCS)* (IEEE, Gainesville, FL, USA, 2021), p. 1.